Journal of Geophysical Research: Biogeosciences

Extensive nitrogen loss from permeable sediments off North-West Africa

Sarah Sokoll[1,2], Gaute Lavik[1], Stefan Sommer[3], Tobias Goldhammer[2], Marcel M. M. Kuypers[1], and Moritz Holtappels[1,2,4]

[1]Max Planck Institute for Marine Microbiology, Bremen, Germany, [2]MARUM-Centre for Marine Environmental Sciences, University of Bremen, Bremen, Germany, [3]GEOMAR Helmholtz Centre for Ocean Research, Kiel, Germany, [4]Alfred Wegener Institute, Helmholtz Centre for Marine and Polar Research, Bremerhaven, Germany

Abstract The upwelling area off North-West Africa is characterized by high export production, high nitrate and low oxygen concentration in bottom waters. The underlying sediment consists of sands that cover most of the continental shelf. Due to their permeability sands allow for fast advective pore water transport and can exhibit high rates of nitrogen (N) loss via denitrification as reported for anthropogenically eutrophied regions. However, N loss from sands underlying naturally eutrophied waters is not well studied, and in particular, N loss from the North-West African shelf is poorly constrained. During two research cruises in April/May 2010/2011, sediment was sampled along the North-West African shelf and volumetric denitrification rates were measured in sediment layers down to 8 cm depth using slurry incubations with ^{15}N-labeled nitrate. Areal N loss was calculated by integrating volumetric rates down to the nitrate penetration depth derived from pore water profiles. Areal N loss was neither correlated with water depth nor with bottom water concentrations of nitrate and oxygen but was strongly dependent on sediment grain size and permeability. The derived empirical relation between benthic N loss and grains size suggests that pore water advection is an important regulating parameter for benthic denitrification in sands and further allowed extrapolating rates to an area of 53,000 km^2 using detailed sediment maps. Denitrification from this region amounts to 995 kt yr^{-1} (average 3.6 mmol m^{-2} d^{-1}) which is 4 times higher than previous estimates based on diffusive pore water transport. Sandy sediments cover 50–60% of the continental shelf and thus may contribute significantly to the global benthic N loss.

1. Introduction

Sediments are important sinks for bioavailable nitrogen (N) in the ocean, as 50–70% of marine N loss is generally attributed to sediments [*Codispoti*, 2007; *Codispoti et al.*, 2001; *Gruber*, 2004]. The continental shelves play a key role in benthic N loss, removing 80–100 Tg N yr^{-1} [*Bohlen et al.*, 2012; *Middelburg et al.*, 1996] of which the majority (>75%) is attributed to denitrification, i.e., the reduction of nitrate (NO$_3^-$) to dinitrogen gas (N$_2$). Anammox, the anaerobic oxidation of ammonium (NH$_4^+$) to N$_2$, is of less importance in shallow coastal waters [*Dalsgaard et al.*, 2005]. To date, the vast majority of N-loss measurements are from muddy sediments where solutes are mainly transported by diffusion [*Devol*, 2015, and references therein; *Nielsen*, 1992; *Seitzinger*, 1988]. These measurements provide the basis for empirical and diagenetic models currently used to estimate global benthic N loss [*Bohlen et al.*, 2012; *Middelburg et al.*, 1996; *Seitzinger and Giblin*, 1996; *Soetaert et al.*, 1996]. Assuming diffusive transport, these models are constrained by bottom water concentrations of NO$_3^-$ and oxygen (O$_2$) and by the flux of organic matter (OM) to the seafloor, which is usually provided as a function of primary production and water depth.

However, 50–60% of the continental shelves are covered with sandy sediments [*Emery*, 1968; *Huettel et al.*, 2014] which are permeable and allow for advective pore water flow. Advective solute transport is independent of concentration gradients, and its efficiency in sands is increased by up to 2 orders of magnitude compared to molecular diffusion [*Huettel et al.*, 2003]. Sandy sediments are indicative of strong bottom water currents and rapid organic matter decay that hinder the accumulation of organic matter and fine grained sediments. The low OM content of less than 1% was often misinterpreted as indicator for a low benthic activity until a growing number of studies caused a paradigm shift showing that sands can act as filter systems, in which retained organic matter is decomposed at high rates [*Boudreau et al.*, 2001; *Huettel and Rusch*, 2000]. In sands the active bacterial community is attached to the sand grains to withstand abrasion

and pore water advection, and cell abundance was found proportional to the available grain surface area [*DeFlaun and Mayer*, 1983]. The grain size distribution of the sediment determines the permeability [*Krumbein and Monk*, 1943], i.e., the ability of the sediment to allow fluid flow in the pore space along pressure gradients. In subtidal areas the pressure gradients are forced by the interaction of seabed topography and bottom water currents [*Santos et al.*, 2012b], which results in highly variable mass transport and complicates reliable flux measurements since common chamber and core incubations cannot reproduce the natural hydrodynamic condition. Pressure gradients are further induced by the pumping activity of benthic infauna causing pore water flow and transport of reactive solutes to greater sediment depths [*Meysman et al.*, 2006a; *Volkenborn et al.*, 2010].

The fundamentally different mode of transport of organic matter and electron acceptors in sands is increasingly accounted for in a number of recent studies using flow through reactors [*Rao et al.*, 2007] and/or depth-resolving volumetric rate measurements that can be integrated down to the penetration depth of the limiting substrate to derive a flux [*de Beer et al.*, 2005; *Polerecky et al.*, 2005]. These studies report high areal N loss of up to 5 mmol N m^{-2} d^{-1} in the Wadden Sea [*Gao et al.*, 2012, 2010; *Marchant et al.*, 2014], the South Atlantic Bight [*Rao et al.*, 2007, 2008], the Gulf of Mexico [*Gihring et al.*, 2010], and Eastern Australia [*Evrard et al.*, 2012; *Kessler et al.*, 2012; *Santos et al.*, 2012a]. The high rates indicate that sandy sediments play an important role in benthic N loss, especially in eutrophied coastal areas where benthic N removal counteract the anthropogenic N input from rivers and atmospheric deposition [*Gruber and Galloway*, 2008]. To date, the number of N-loss estimates from sandy sediments is still limited, and many sandy shelf systems have not been investigated at all. Moreover, the common empirical and diagenetic models for benthic N loss [*Bohlen et al.*, 2012; *Middelburg et al.*, 1996; *Soetaert et al.*, 2000] are not appropriate for permeable sediments as they implicitly assume transport along concentration gradients but do not consider the abiotic regulation of advective pore water flux.

The North-West African shelf is characterized by large areas of sandy sediments, especially off Senegal and Mauritania [*Diester-Haass and Müller*, 1979; *Holz et al.*, 2004]. Although they underlie one of the most productive upwelling systems with a high primary production of 0.33 Gt C yr^{-1} [*Carr*, 2002], sands are found ubiquitous from shallow coastal waters down to 500 m depth. In contrast to other Eastern Boundary upwelling areas, water masses are permanently oxic with concentrations above >22 μmol L^{-1} [*Helly and Levin*, 2004], and therefore, N loss does not occur in the water column. However, the high organic matter export in combination with low O$_2$ and high NO$_3^-$ in bottom waters (>15 μmol L^{-1}) [*Dale et al.*, 2014] provide ideal conditions to fuel benthic denitrification, possibly at comparable rates to those found in anthropogenically eutrophied coastal waters [*Gao et al.*, 2012]. Currently, the sediments of the NW African shelf (0°–45°N, water depth < 200 m, 418,000 km^2) are believed to be responsible for an N loss of 1.7 × 10^{11} mol N yr^{-1} and thus for 0.5–1.5% of global marine N loss [*Seitzinger and Giblin*, 1996]. However, this estimate results from an empirical model based on measurements from other shelf systems that do not consider the role of advective transport in permeable sediments.

Here we present measurements of benthic denitrification and anammox using ^{15}N incubation experiments. Areal N loss was determined at 16 stations off Senegal and Mauritania at water depths ranging from 50 to ~3000 m. For permeable sediments at 50 to 500 m water depth an empirical relation between areal denitrification rates and median grain size was found and used to extrapolate N loss to the entire Mauritanian and Senegalese shelf area.

2. Material and Methods

2.1. Water Column Sampling and Nutrient Analysis

Sampling was conducted during two cruises to the Western African Shelf (Figures 1a and 1b). In April 2010, a cruise to Cape Blanc off the border between Mauritania and Western Sahara was conducted with R/V *Poseidon* (P398, Table 1). In March/April 2011, a cruise went to the shelf off Senegal and Mauritania with R/V *Maria S. Merian* (MSM17/4, Table 1). At 68 stations, dissolved oxygen, salinity, and temperature were measured in the water column with a conductivity-temperature-depth (CTD) system, equipped with an oxygen sensor (Sea Bird Electronics). Oxygen concentrations were calibrated against Winkler titration. Water samples for nutrient analysis were taken with a CTD Rosette. Ammonium and nitrite were measured fluorometrically and photometrically on board [*Grasshoff and Johannsen*, 1972; *Holmes et al.*, 1999].
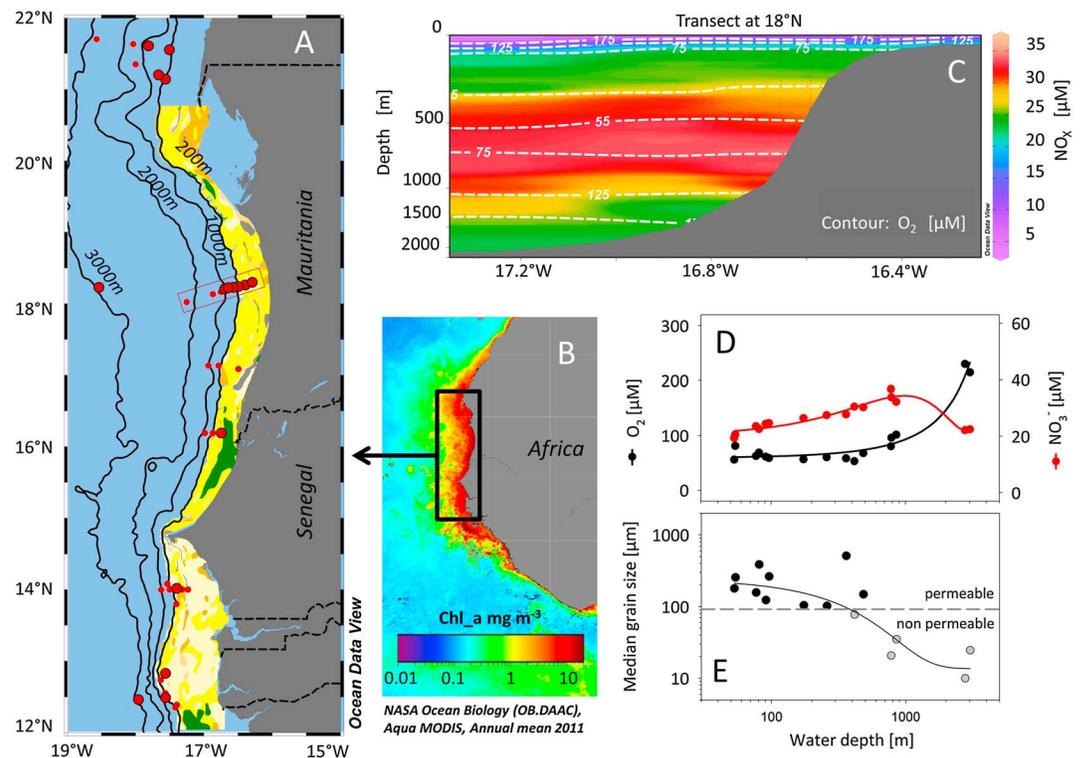
Figure 1. (a and b) A total of 16 stations was sampled to determine benthic N loss at the continental margin off North-West Africa. Big dots denote sediment station; small dots denote other CTD stations. Sediment properties down to 200 m water depth were taken from detailed sediment maps (see text) and show the dominance of sands. Yellow to brown colors denote coarse (>500 μm), medium (315–500 μm), fine (160–315 μm), and very fine sands (63–160 μm), and green colors denote mud (50% smaller than 63 μm). (Figure 1b) Annual composite of chlorophyll *a* concentration in 2011 derived from satellite data (Aqua MODIS (Moderate Resolution Imaging Spectroradiometer)). (c) A transect across the oxygen minimum zone at 18°N shows the depletion of oxygen (isolines) and the accumulation of nitrate (color) at specific depths. (d) For the 16 sediment stations, bottom water nitrate and oxygen are plotted as a function of water depth. Lines display exponential fit. (e) For the same stations, median grain size of the surface sediment is shown as a function of water depth. Black and grey dots denote permeable and nonpermeable sediments, respectively.

Samples for nitrate measurements were immediately frozen and stored at −20°C for later determination with an autoanalyzer (TRAACS 800, Bran & Luebbe) in an onshore laboratory.

2.2. Sediment Sampling and Pore Water Analysis

At 16 stations (Table 1) sediment samples were taken either with a multicorer (MUC) or during benthic lander deployments [*Dale et al.*, 2014] and immediately processed after retrieval. Procedures of pore water extraction and analysis for cruise MSM 17/4 have been published elsewhere [*Dale et al.*, 2014]. Briefly, pore water was extracted either by rhizons® (cruise P398, MSM17/4) or by slicing the sediment in an argon atmosphere (MSM17/4). Sediment slices were subsequently centrifuged at maximum 4500 G for 20 min and the supernatant pore water filtered with 0.2 μm cellulose acetate Nuclepore® filters. Aliquots of pore water were diluted with O_2-free artificial seawater prior to analysis when necessary. Ammonium (NH_4^+) was measured according to *Grasshoff et al.* [1999] and nitrate (NO_3^-) was measured chromatographically or with a chemoluminescence NO_x analyzer (Thermo Environmental Instruments Inc.) after *Braman and Hendrix* [1989]. Porosity was calculated from the weight loss of known volumes of wet sediment during freeze drying, assuming a dry solid density of 2.5 g cm^{-3}, or from the difference in Cl$^-$ concentrations measured in pore water and freeze-dried sediments (only cruise P398). Concentrations of total carbon and nitrogen were determined by combustion/gas chromatography (Carlo Erba NA-1500 CNS analyzer) of dried sediment samples. Total inorganic carbon was measured with a Coulometer (CM-5130, UIC Inc.) and subtracted from total carbon to derive organic carbon content (C_{org}) of the sediment.

Table 1. Station Parameters Sorted for Increasing Water Depths[a]

Cruise	Station	Latitude	Longitude	Depth	O₂	NO₃⁻	Porosity	Grain Size	Sand Fraction	Permeability	Sediment Classification	C_ORG	NO_x Depth	Denitrification Rates Surface	Mean	Flux (Integrated Rates) Denitrification	Anammox	Total	Denitrification
(-)	(-)	(°N)	(°W)	(m)	(µmol L⁻¹)	(µmol L⁻¹)	(-)	(µm)	(%)	(m²)	(-)	(%)	(cm)	(nmol N cm⁻³ d⁻¹)	(nmol N cm⁻³ d⁻¹)	(mmol N m⁻² d⁻¹)	(mmol N m⁻² d⁻¹)	(mmol N m⁻² d⁻¹)	(%)
											Permeable Sediments								
MSM17	554	18°17.4	16°19.2	53	55.9	19.4	0.60	179.4	83.0	3.4E−12	fine sand	0.81	1.0	238.3	219.9	2.38	0.04	2.43	98
MSM17	342	12°50.0	17°33.8	54	81.0	20.6	0.39	256.2	98.4	2.0E−11	fine sand	0.11	ND	215.3	191.6	ND	ND	ND	ND
MSM17	529	18°16.3	16°24.0	77	62.6	23.6	0.58	157.5	85.9	4.1E−12	fine sand	0.45	1.5	258.9	226.9	3.88	0.12	4.00	97
MSM17	366	13°60.0	17°24.0	81	68.5	22.6	0.55	387.1	96.7	2.6E−11	medium sand	0.58	2.5	238.1	222.1	5.88	2.10	7.98	74
MSM17	380	16°11.5	16°45.0	91	61.2	24.4	0.54	123.2	82.3	4.4E−12	very fine sand	0.73	1.0	192.5	227.6	1.92	0.52	2.45	79
MSM17	410	18°15.3	16°27.0	96	58.8	24.7	0.60	262.8	88.1	7.1E−12	fine sand	0.86	1.5	282.9	360.9	4.24	0.54	4.78	89
MSM17	552	18°14.3	16°31.0	174	56.6	26.4	0.70	104.5	72.3	2.9E−12	very fine sand	1.50	0.5	261.9	230.1	1.31	0.20	1.51	87
P398	14105	21°08.9	17°35.6	259	60.2	27.5	0.78	102.3	74.2	3.3E−12	very fine sand	1.97	1.5	187.3	173.9	2.81	0.69	3.50	80
P398	14107	21°10.2	17°38.7	361	58.1	27.8	0.73	513.0	95.8	6.9E−11	coarse sand	1.67	7.0	111.8	129.4	9.15	ND	9.15	ND
P398	14102	21°34.2	17°31.5	485	67.8	30.3	0.68	149.1	86.2	4.8E−12	very fine sand	1.15	4.0	28.1	50.4	2.60	1.46	4.05	64
											Impermeable Sediments								
MSM17	449	18°12.5	16°35.6	420	53.0	30.5	0.66	77.5	59.6	1.4E−12	very fine sand	1.28	0.5	394.1	337.9	1.97	0.86	2.83	70
MSM17	330	12°28.3	17°35.3	781	80.2	36.7	0.91	20.7	26.3	1.4E−14	mud	3.54	0.5	872.8	498.8	4.36	0.19	4.55	96
MSM17	496	18°11.3	16°39.3	787	95.9	33.8	0.85	ND	ND	ND	ND	ND	0.5	154.0	124.5	0.77	0.09	0.86	89
P398	14103	21°36.2	17°48.2	855	101.4	32.2	0.84	35.0	28.8	1.5E−13	mud	3.82	4.0	80.6	71.4	3.08	1.22	4.31	72
MSM17	326	12°26.3	17.58.8	2778	230.1	22.2	0.92	9.9	3.9	8.7E−15	mud	2.36	ND	13.4	63.4	ND	ND	ND	ND
MSM17	522	18°13.0	18°32.0	3024	214.7	22.5	0.82	24.5	27.2	1.7E−14	mud	1.02	5.5	2.3	16.1	0.78	1.38	2.16	35

[a]Water column properties: water depth, bottom water concentrations of O_2 and NO_3^-. Sediment properties: porosity (0–2 cm), median grain size (0–2 cm), % sand (>63 µm), permeability (0–2 cm), organic carbon content (0–2 cm), NO_x penetration depth. Rate measurements: denitrification rates (0–2 cm), average denitrification of all layers, integrated rates (flux): denitrification, anammox, and total flux, % denitrification. ND, not determined.

2.3. Grain Size Analysis and Permeability Calculation

From the upper layer (0–2 cm), sediment was collected for grain size analysis. Grain size distribution was measured with a Laser Diffraction Particle Size Analyzer (Beckman Coulter) LS200 for 92 size classes from 0.4 to 2000 μm. Measurements were performed after pretreatment of the samples with H_2O_2 to remove organic compounds. The fraction of grain sizes >63 μm was denoted as sand. The lognormal distribution of the grain size diameter was used to calculate sediment permeability using the empirical relationship of *Krumbein and Monk* [1943]:

$$k = 760 \, d^2 \exp(-1.31 \, \sigma) \tag{1}$$

where k is the permeability in darcys, d is the mean grain diameter in mm, and σ is the standard deviation of the Φ distribution ($\Phi = -\log_2(d)$). Permeability was converted from darcy to the more common unit m^2. Sediments with a median grain diameter above 100 μm and a permeability above $2 \times 10^{-12} \, m^2$ were classified as permeable sands [*Huettel and Gust*, 1992].

2.4. ^{15}N Incubation Experiments

Sediments for incubation experiments were sampled by a MUC using plastic liners with an inner diameter of 10 cm. Sediment cores were cut in 2 cm layers to a depth of 6, 8, or 12 cm and prepared for incubation in air tight bags as described in detail elsewhere [*Gao et al.*, 2010; *Sokoll et al.*, 2012]. Briefly, the sediment slices were transferred to air tight bags, which were carefully sealed. Degassed bottom water (200–300 mL) was added with a syringe through a glass port, and any residual gas phase was carefully removed. At two stations (342 and 366) incubations were performed with nondegassed bottom water (70–80 μmol O_2 L^{-1}). ^{15}N substrate (Sodium-^{15}NO$_3$, ^{15}NH$_4$-Sulfate, Sigma-Aldrich) was added with a 1 mL syringe through the stopper into the bags to final concentrations of 60–90 μmol L^{-1} (cruise MSM17/4) and 230 μmol L^{-1} (cruise P398). For denitrification experiments ^{15}NO$_3^-$ was added, while ^{15}NH$_4^+$ and ^{14}NO$_2^-$ were added to detect anammox. Allylthiourea (ATU, 86 μmol L^{-1}) was added to anammox experiments to exclude ammonia oxidation [*Ginestet et al.*, 1998] from any remaining O_2. The bags were incubated in the dark and gently mixed prior to subsampling.

After 0, 3, 6, 12, and 24 h (cruise MSM17/4) and 0, 6, 12, 24, and 36 h (cruise P398), subsamples of 6 mL were taken with a syringe, transferred to gas tight glass vials (Exetainer^{TM}, Labco) and killed by adding 100 μL of saturated HgCl$_2$ solution. The Exetainers were stored at room temperature in the dark until further processing. A headspace of 1 mL Helium was introduced into the Exetainers before measuring ^{15}N-N$_2$ concentrations using gas chromatography-isotopic ratio mass spectrometry (VG Optima Micromass) as described by *Holtappels et al.* [2011]. A linear increase of ^{15}N-N$_2$ was observed from the start. At some stations, the production of ^{15}N-N$_2$ leveled off after 6–24 h due to substrate limitation so that N$_2$ production rates were calculated from the linear increase of ^{29}N$_2$ and ^{30}N$_2$ over the first 6–24 h of the incubation. Denitrification rates (D) were calculated according to *Thamdrup and Dalsgaard* [2002]:

$$D = \frac{p^{30}N_2}{\left(F_{NO_3^-}\right)^2} \tag{2}$$

where $p^{30}N_2$ denotes the ^{30}N$_2$ production measured in the denitrification experiment and F_{NO3-} is the ratio of ^{15}NO$_3^-$ over the total NO$_3^-$ in the slurry. Anammox rates (A) were calculated according to the following:

$$A = \frac{p^{29}N_2}{\left(F_{NH_4^+}\right)^2} \tag{3}$$

where $p^{29}N_2$ denotes the ^{29}N$_2$ production measured in the anammox experiment and F_{NH4+} is the ratio of ^{15}NH$_4^+$ over the total NH$_4^+$ in the slurry. The labeling percentage (F_N) of either nitrate or ammonium, ranged between 0.96 and 0.60. All denitrification and anammox rates were calculated as rates of N loss per volume of wet sediment.

The bags were incubated at in situ temperature during cruise MSM17/4. Unfortunately, temperature control in the laboratory did not work at four stations during cruise P398 and the incubations proceeded at 20°C, which was ~8°C higher than the in situ temperatures. To correct for the higher temperatures, we used the Arrhenius equation [*Rysgaard and Glud*, 2004]:

$$k(T') = k(T) \, \exp(\beta \, (T' - T)/(T \, T')) \tag{4}$$

where T is the incubation temperature, T' is the in situ temperature, and k is the rate. Further, $\beta = E_a/R$ where

R is the gas constant ($8.314 \, J \, k^{-1} \, mol^{-1}$) and E_a is the activation energy for which values of $60.6 \, kJ \, mol^{-1}$ (denitrification) and $51.0 \, kJ \, mol^{-1}$ (anammox) were taken from *Rysgaard and Glud* [2004].

Due to the addition of labeled N substrate, the measured rates are treated as potential rates when no pore water NO_x was found, even though the immediate onset of $^{15}N\text{-}N_2$ production suggests that an active denitrifier/anammox community was present. To calculate areal N-loss rates, we considered only the volumetric rates from sediment depths where pore water NO_x was measured. Areal N-loss rates were derived for each station by integrating the volumetric rates over NO_x penetration depths. In parallel, during cruise MSM17 benthic landers were deployed at five stations (410, 449, 496, 552, and 554) nearby the MUC sampling sites for this study. Areal denitrification rates were estimated from in situ chamber measurements [*Dale et al.,* 2014] and were used to evaluate the integration approach.

2.5. Sediment Distribution

To estimate the areal distribution of sand on the North-West African shelf, detailed maps of shelf sediments between latitude 12°–21°N and water depths of 10–200 m [*Domain*, 1977; *Domain and Richer de Forges*, 1985] were digitized using the mapping software Global Mapper© (Blue Marble Geographics, USA). The sediment classification (Figure 1a) was adopted from the original maps where the median grain size was used to distinguish between coarse sand (2000–500 μm), medium sand (315–500 μm), fine sand (160–315 μm), and very fine sand (63–160 μm). Areas with muddy sediment were characterized by median grain sizes smaller than 63 μm.

3. Results

3.1. Water Column

From a total of 68 CTD stations, water column O_2 and NO_3^- concentrations were determined showing a pronounced O_2 deficit zone with concentrations of less than 75 μM between 50 and 700 m depth and with minimum concentrations of 50 μM situated at 400 m water depth (see example for transect at 18°N, Figure 1c). Below 1500 m depth, O_2 concentration increased to above 200 μM. Except for the upper mixed layer (0–30 m), NO_3^- concentrations were well above 15 μM and increased with depth to maximum concentrations of more than 30 μM between 500 and 1000 m depth. Similar trends were observed for the bottom water concentration of O_2 and NO_3^- at the 16 stations where N-loss experiments were performed (Figure 1d and Table 1). In agreement with satellite images (Figure 1b), chlorophyll concentrations in the upper mixed layer ranged from 0.4 to 4 μg L^{-1} showing increased concentrations on the shelf at water depths of 100 m to 1000 m.

3.2. Sediments

Sediment porosity increased with water depth (Table 1), whereas median grain diameter and permeability decreased with water depth (Table 1 and Figure 1e). For sediments between 50 m and 400 m water depth, porosity ranged between 0.4 and 0.8, and sediments below ~800 m were characterized by higher porosities (0.8 to 0.9). Median grain diameters of 100–500 μm and sand content of 86% on average were found at 10 stations in shallow water depths of less than 500 m. The corresponding permeabilities ranged from 3×10^{-12} to $7 \times 10^{-11} \, m^2$, so that the sediment at these stations was classified as permeable. Only one station in shallow waters (<500 m) was considered impermeable (station 449 at 416 m). All remaining stations in deeper waters (>500 m) revealed median grain diameters between 9 and 77 μm, a mean sand content of 29% with corresponding permeabilities of less than $2 \times 10^{-12} \, m^2$, so that sediments were classified as impermeable. Organic carbon content (C_{org}) in the surface layer of the sediment (0–2 cm) was positively correlated with porosity (R^2: 0.71, $p < 0.0001$). C_{org} was low (0.1–0.8%) in shallow water depths down to 100 m, increased with water depth to 3.8% at ~800 m, and decreased again to 1.1–2.5% at ~3000 m depth. Combined nitrate and nitrite concentrations (NO_x) in the pore water decreased with sediment depth (Figure 2), with the exception of the deep station 522 (~3000 m), where a NO_x maximum of 36 μmol L^{-1} was found at 1.5 cm. At four stations NO_x was detectable to depths of 4–6 cm, while at all other stations nitrate was depleted within the 0.5–2.5 cm (Table 1 and Figure 2).

3.3. Denitrification and Anammox Rates

The N loss due to denitrification and anammox was measured in slurry incubation experiments amended with ^{15}N compounds. The rates were calculated from the linear increase of $^{15}N\text{-}N_2$ concentrations over time.
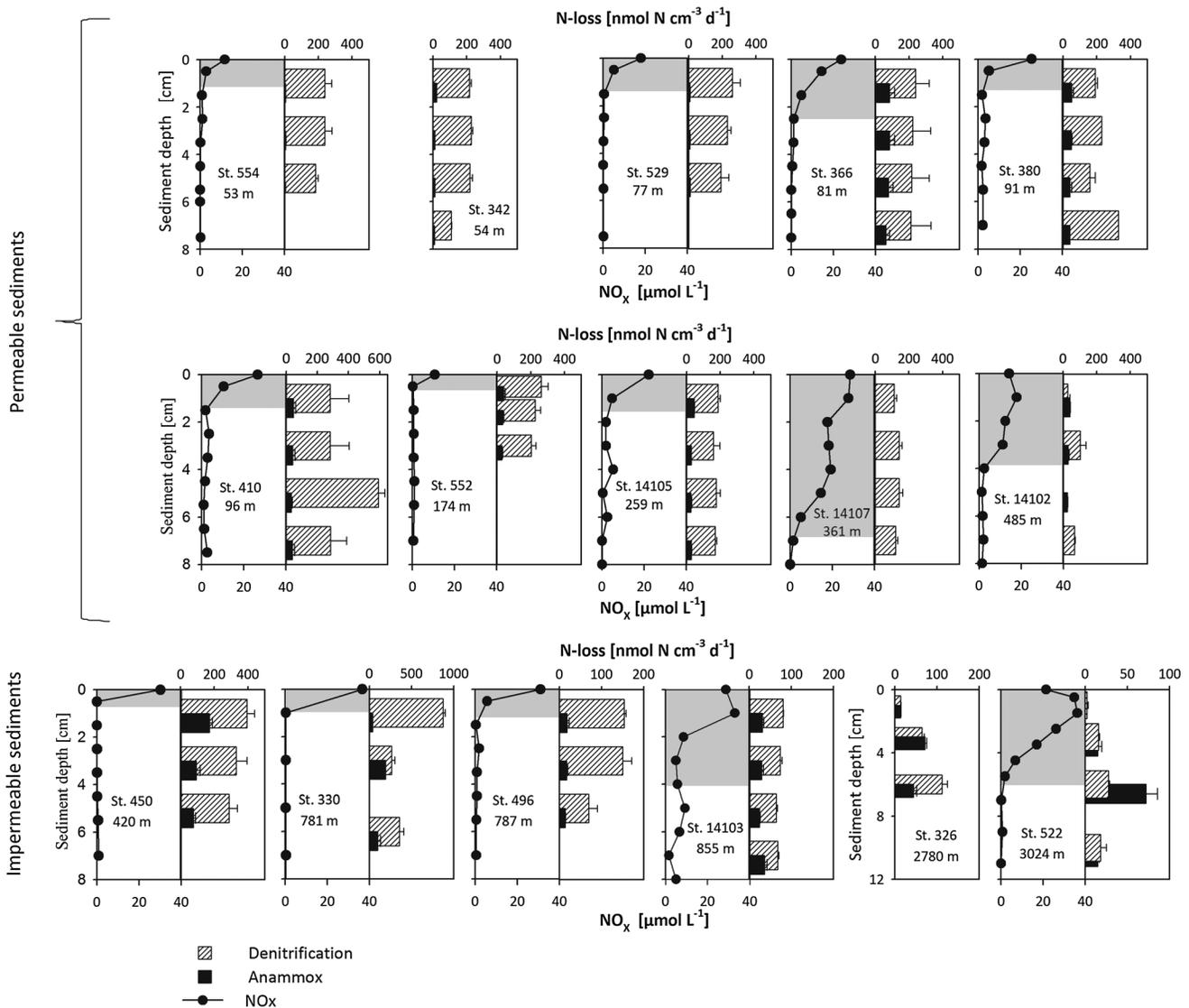
Figure 2. Pore water profiles of NO_x (left panels) and N-loss rates (right panels) are shown for (top) 10 permeable stations and (bottom) 6 impermeable stations. Stations are sorted by water depth. Grey areas mark the NO_x penetration depth. Please note the different scaling of N-loss rates and sediment depth among the impermeable stations. Anammox incubations at station 14107 failed. Incubations at stations 342 and 366 were performed with nondegassed bottom water (70–80 μmol O_2 L^{-1}).

The production of ^{15}N-N_2 started immediately within the first time interval, and only 2 out of 107 incubations showed a slight exponential increase (stations 326 and 522, at 0–2 cm). At stations with permeable sediments, denitrification rates ranged from 150 to 250 nmol N cm^{-3} d^{-1} (Figure 2, top). Only the permeable sediments in 485 m water depth (station 14102) showed lower denitrification rates of 50 nmol N cm^{-3} d^{-1}. The denitrification rates in different sediment layers were similar and did not follow a trend, so that most stations with permeable sediments showed a variability of less than 15% between depth layers. In permeable sediments, anammox rates were low (4 to 80 nmol N cm^{-3} d^{-1}) with an average N-loss contribution of 16%. No trend with sediment depth was observed.

Between stations with impermeable sediments, N-loss rates were more variable (Figure 2, bottom), ranging from 10 to 870 nmol N cm^{-3} d^{-1} for denitrification and from 4 to 190 nmol N cm^{-3} d^{-1} for anammox. The N-loss contribution of anammox was on average 26%. Especially at the deep stations (stations 326 + 522) the contribution of anammox was high and in some cases exceeded those of denitrification. At these stations a clear vertical zonation of the N-loss rates was observed, and consequently, they varied between depth layers by more than 65%.
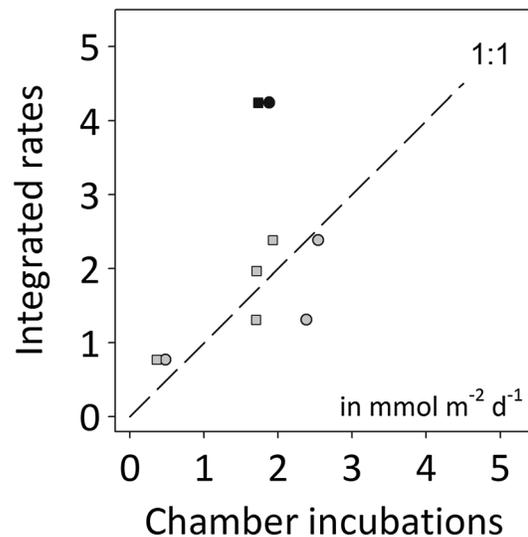
Figure 3. Comparison of areal denitrification rates derived from chamber incubations [*Dale et al.*, 2014] and from rate integration down to the NO_x penetration depth (this study). Squares and circles denote incubations from chambers 1 and 2, respectively. Grey symbols denote sediments with very low permeability ($<3.4 \times 10^{-12}$ m^2), and black symbols denote sediments with a relatively high permeability of 7×10^{-12} m^2.

At two stations (342 and 366) the sediment was incubated with oxic bottom water. The rates of $\sim$220 nmol N cm^{-3} d^{-1} were comparable to those from incubations with degassed bottom water. The production of ^{15}N-N_2 started immediately and did not increase over time suggesting that the low O_2 concentrations in the bottom water ($\sim$25% air saturation) did not inhibit denitrification. Therefore, volumetric rates of denitrification and anammox were integrated over the full NO_x penetration depth (shaded area in Figure 2 and Table 1) to derive areal N-loss rates (i.e., N-N_2 fluxes). The case of potential inhibition of N loss by bottom water O_2 is discussed in section 4.4.

3.4. N-Loss Fluxes

At two stations (stations 326 and 342), NO_x profiles were not determined, and hence, the areal N loss could not be calculated. To validate the integration approach, areal denitrification rates were compared to flux measurements from benthic chamber incubations published previously by *Dale et al.* [2014]. At four stations with either impermeable or very fine sands areal denitrification rates agree well with measurements of *Dale et al.* [2014] (Figure 3). Only the chamber incubations of coarser grained permeable sediment (station 410) gave estimates of 1.7–1.9 mmol N m^{-2} d^{-1}, which is less than half of what was found in this study (4.2 mmol N m^{-2} d^{-1}). This discrepancy can be explained by the suppressed hydrodynamic forcing in the incubation chamber, which decreases the advective NO_x transport into the permeable sediments and compromises chamber incubations especially for such high permeabilities [*Janssen et al.*, 2005].

Across all stations, areal N loss ranged from 0.8 to 9.1 mmol N m^{-2} d^{-1}. Denitrification was the dominant N-loss process with high contributions in permeable sediments (Figure 4a) and is analyzed in the following in more detail. The areal denitrification rates of all investigated sites varied by more than 1 order of magnitude. This variability could not be related to water depth or bottom water NO_x (Figures 4b and 4c). Also, no significant correlation was found for volumetric rates, bottom water oxygen, or benthic organic carbon content ($p > 0.6$, 0.09, and 0.7, respectively). However, when separating the data into permeable and impermeable sediments, we found that median grain size could explain 92% of the variability of areal denitrification rates in permeable sediments (Figure 4d). Consequently, the areal rates were also well described by sediment permeability calculated from grain size (equation (1)) using the logarithmic function $y = 2.14 \ln(x) + 58.9$ (R^2: 0.91 and $p < 0.0001$). For the permeable sites, a significant correlation was also found between median grain size and NO_x penetration depth (Figure 4f). However, the variability of the volumetric denitrification rates could not be explained by the grain size ($p > 0.6$) but showed a significant trend with water depth (Figure 4e).
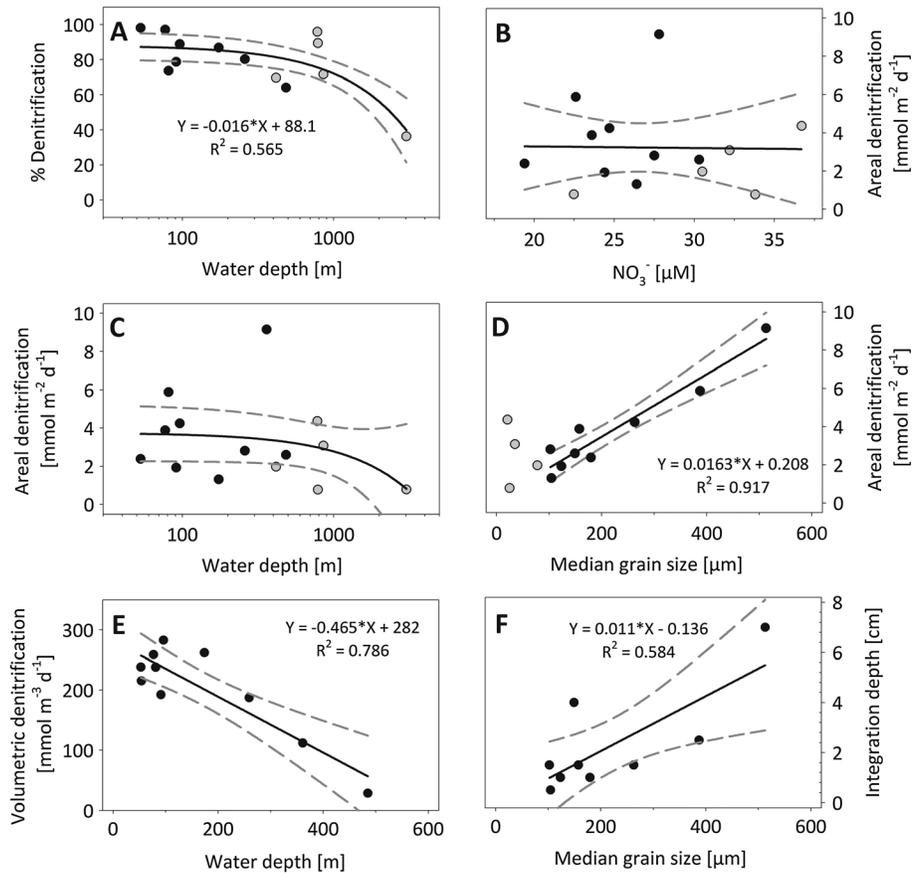
3.5. Regional N Loss

Median grain size determines the permeability of the sediment (see equation (1)) and reflects the strength of prevailing bottom water currents. Indeed, we found strong bottom water currents of up to 20 cm s^{-1} measured with an acoustic Doppler velocimeter even at water depths of 240 m (near station 552, data not shown). Besides infauna pumping, interaction of strong currents with sediment topography is the most important driver for pressure gradients and thus for the forcing of pore water flow. In summary, this makes median grain size a strong proxy for advective pore water flow and, apparently, also for areal denitrification which is usually limited by NO_x transport. The observed linear relation of areal denitrification rates and grain size (Figure 4d) was applied to extrapolate rates to the entire shelf area. Using a detailed sediment map (Figure 1a, 12–21°N, 53,716 km^2), shelf sediments were divided into coarse sand (4493 km^2), medium sand (1790 km^2), fine sand

Figure 4. (a) Contribution of denitrification to total N loss at all stations as a function of water depth. Areal denitrification rate of all stations as a function of (b) bottom water NO_x and (c) water depth. (d) Areal denitrification rate in permeable sediments as a function of median grain size. (e) Volumetric denitrification rate in permeable sediments as a function of water depth. (f) NO_x penetration depth as a function of median grain size. Black and grey dots denote permeable and impermeable stations, respectively. Dashed grey lines mark the 95% confidence interval. Equations are given only for significant linear regressions ($p < 0.05$).
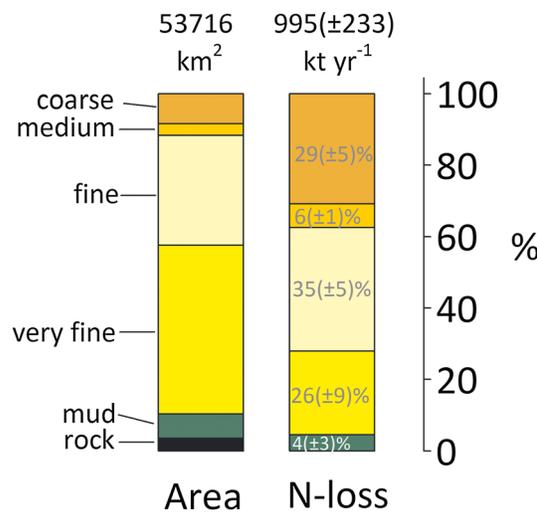
Figure 5. The relative abundance of sediment types in the investigated area and their contribution to the estimated total N loss.

(16,517 km^2), very fine sand (25,392 km^2), mud (3625 km^2), and rock (1899 km^2). For rocky seabed, zero denitrification was assumed, whereas for muddy sediments an average denitrification of 2.2 ($\pm$1.5) mmol m^{-2} d^{-1} was calculated from the measurements at stations with impermeable sediments. For coarse, medium, fine, and very fine sands, an areal denitrification rate of 12.4 ($\pm$2.4), 6.8 ($\pm$1.0), 4.1 ($\pm$0.6), 2.0 ($\pm$0.8) mmol m^{-2} d^{-1} was derived from the linear function and the respective 95% confidence interval (Figure 4d). In summary, denitrification of the entire area was 1.95 ($\pm$0.5) $\times 10^8$ mol N d^{-1} and the spatially averaged denitrification was 3.6 ($\pm$0.9) mmol m^{-2} d^{-1}. Assuming similar conditions throughout the year, a total of 7.1 ($\pm$1.7) $\times 10^{10}$ mol N yr^{-1} is denitrified, which is equivalent to 996 ($\pm$233) kt N yr^{-1}. Sands with median grain sizes larger than 160 μm (fine,

medium, and coarse sands) contribute 70% (±11%) of the total denitrification although they cover only 42% of the entire area (Figure 5). In contrast, sediments with median grain size of less than 160 μm make up 47% (very fine sand) and 7% (mud) of the area but contribute only 26% (±9.5%) and 4% (±2.8%) to the total denitrification.

4. Discussion

4.1. Permeable Sediments

Permeability was estimated to allow classification into permeable and impermeable sediments. Permeability was calculated from grain size, and the model of *Krumbein and Monk* [1943] was chosen because the estimates were conservative compared to other models from, e.g., Carman-Kozeny, Blake-Kozeny, and Rumpf-Gupte, (summarized by *Boudreau* [1997]) which gave higher permeabilities throughout. In addition, permeability was measured at two occasions to validate the calculations. As we were not prepared for such high sand content a falling head permeability setup was constructed on board and permeabilities of $1.1 \times 10^{-11}\,m^2$ (station 366) and $9.7 \times 10^{-12}\,m^2$ (station 410) were measured, which is in the range of the calculated values (Table 1). The high sand content of $86 \pm 9\%$ further indicates that permeable sediments had indeed a high potential for advective pore water flow.

To distinguish between permeable and impermeable sediments, a boundary value of ~$2 \times 10^{-12}\,m^2$ was adapted from *Huettel and Gust* [1992] who examined advective pore water transport for pressure gradients of the order of $1\,Pa\,cm^{-1}$. Applying Darcy's law and assuming permeabilities of $2 \times 10^{-12}\,m^2$, a pressure gradient of $1\,Pa\,cm^{-1}$ is sufficient to drive a pore water flow of ~$1\,\mu m\,s^{-1}$ which outcompetes diffusive transport already over distances of >2 mm. It was shown in several flume experiments and model studies that pressure gradients of this magnitude are induced by small-scale topographies such as sediment ripples or biogenic mounds that interact with currents of the order of $10\,cm\,s^{-1}$ [*Ahmerkamp et al.*, 2015; *Janssen et al.*, 2012]. In this study, strong bottom water currents of up to $20\,cm\,s^{-1}$ were observed down to water depths of 240 m (data not shown), which corresponds to the nonaccumulating coarse-grained sediments found in this region.

Bioirrigation, i.e., the pumping of infauna, also induces pressure gradients and pore water flow which significantly enhances the affected sediment volume in permeable sediments compared to cohesive muddy sediments [*Meysman et al.*, 2006a; *Meysman et al.*, 2006b; *Volkenborn et al.*, 2010]. At some stations (e.g., 410 and 450) a rich benthic macrofauna community was observed in the sampled sediment which supports the observation that the faunal richness is increased in the upwelling regions of the North-West African coast [*Le Loeuff and von Cosel*, 1998].

4.2. NO$_x$ in Pore Water

In shallow waters (<500 m), NO$_x$ in pore water was detected down to sediment depths of 1–7 cm, which is comparable to nitrate penetration depths of ~1.5–3.5 cm found in the same region at water depths of 330 and 500 m [*Jaeschke et al.*, 2010]. NO$_x$ penetration depths in permeable sediments showed a significant positive correlation with grain size (Figure 4f, $p < 0.029$) which suggests that coarser grain sizes enhance the NO$_x$ transport due to the increased permeability. In contrast, volumetric N-loss rates control how fast NO$_x$ is consumed and thus showed a significant negative correlation with NO$_x$ penetration depth (R^2: 0.5, $p < 0.04$, not shown).

4.3. Volumetric N-Loss Rates

Denitrification was dominant in permeable sediments at shallow water depths (Figure 2), which corresponds to previous studies describing denitrification as the main N-loss process in permeable sediments [*Gao et al.*, 2012; *Marchant et al.*, 2014]. Strong contribution of anammox to N loss was found only at deeper stations with muddy sediments (Figure 2, stations 522 and 326). At these stations, a stable redox zonation was found. The NO$_x$ profile indicated net NO$_x$ production (nitrification) at 1.5 cm depth while a NO$_x$ sink was indicated at 6 cm depth where N-loss rates were highest. Denitrification and anammox rates at the deep station (20 and 70 nmol N cm^{-3} d^{-1}, station 522) were comparable to rates measured off the Washington margin (41 and 43 nmol N cm^{-3} d^{-1}) at a comparable water depth using the same method [*Engström et al.*, 2009].

At all other stations, especially those with permeable sediments, rates showed no clear trend with sediment depth. Irrespective of the nitrate concentration in the pore water, the potential for immediate denitrification was found down to 8 cm depth, suggesting an occasional NO_x supply by either physical forcing (pore water advection and sediment transport) or biological forcing (bioirrigation and bioturbation), that can be exploited by opportunistic denitrifiers. In comparison to the deep stations (stations 522 and 326), volumetric denitrification rates at all shallower stations (50–350 m water depth) were fivefold to tenfold higher at $220 \pm 62 \, nmol \, N \, cm^{-3} \, d^{-1}$, which is comparable to volumetric rates of $140–545 \, nmol \, N \, cm^{-3} \, d^{-1}$ measured in sediments of the North Sea and the Wadden Sea using slurry incubations with oxic and anoxic water as well as flow through reactors [*Gao et al.*, 2012, 2010; *Marchant et al.*, 2016, 2014].

The difference in activity between stations presumably reflects different NO_x transport conditions, which change from advective pore water transport in permeable and shallow sediments to a diffusion limited transport in cohesive sediments at the deep stations. Increased denitrification may also be stimulated by the flux of labile organic matter. The main parameter controlling the organic matter availability is water depth [*Middelburg et al.*, 1996], which indeed could explain 79% of the variability of the volumetric denitrification rates in permeable sediments (Figure 4e, $p < 0.001$).

4.4. Areal N Loss

Areal N Loss was calculated by integrating volumetric denitrification rates from the sediment surface down to the NO_x penetration depth. The penetration depth of O_2 was not measured, and areal denitrification rates could have been overestimated in case of complete inhibition of denitrification in the oxic layer. However, there is strong evidence that denitrification was not affected by O_2. The bottom waters were deoxygenated, and severe hypoxia (~25% saturation) was found especially at all shallow stations below 500 m water depth. Under such hypoxic conditions, denitrification has been observed many times in the laboratory (see references in *Chen and Strous* [2013]) as well as in marine sediments [*Gao et al.*, 2012; *Marchant et al.*, 2016; *Rao et al.*, 2008]. Indeed, the aerobic bag incubations in our study showed denitrification rates similar to those in anoxic incubations (stations 342 and 366, Figure 2 and Table 1). An immediate onset of the ^{15}N-N_2 production was observed, and the rate of production did not increase with time, i.e., declining O_2 concentrations in the incubations had no effect. This indicates that denitrification was independent of the low O_2 concentrations. Nevertheless, we estimated the relative error for the case of complete inhibition to range between 7% and 26% (see supporting information). The error-corrected values did not affect the quality of the linear regression model and the values scattered within the 95% prediction interval of the original linear regression model (Figure S1 in the supporting information). In summary, our experiments support the approach of integrating denitrification rates over the full NO_x penetration depth and the potential error is within the predicted range of scatter. Moreover, cross validation with benthic chamber incubations showed good agreement of areal denitrification rates for most stations (Figure 3).

On the other hand, the NO_x penetration depth in permeable sediments may have been underestimated. In the retrieved cores, hydrodynamic forcing of the advective NO_x flux is cutoff, and consequently, the denitrification rates will cause an upward shift of the NO_x penetration depth until the pore water is sampled. As a result, the rate integration over the full NO_x penetration depth leads to rather conservative N-loss estimates.

Areal denitrification rates in permeable sediments ranged between 1 and $9 \, mmol \, N \, m^{-2} \, d^{-1}$, which is higher than rates measured in the South Atlantic Bight of $0.25–1.5 \, mmol \, N \, m^{-2} \, d^{-1}$ [*Rao et al.*, 2007], but comparable to rates measured at the Australian coast (up to $16.1 \, mmol \, N \, m^{-2} \, d^{-1}$) [*Santos et al.*, 2012a] and in the intertidal Wadden Sea ($3.5–7.2 \, mmol \, N \, m^{-2} \, d^{-1}$) [*Gao et al.*, 2012]. The large variability of areal denitrification could not be explained by any of the measured parameters except for grains size. A robust correlation between grain size and areal rates was found even when treating the data from the two cruises separately. Slopes of 0.015 and 0.016 and R^2 of 0.85 and 0.98 (for the 2010 and 2011 cruise, respectively) were similar to those of the entire data set (Figure 4d). How and under which circumstances grain size may control benthic fluxes is explained in the following.

4.5. Regulation of Areal Denitrification Rates in Permeable Sediments

In diffusion-controlled sediments, the flux of a reactive solute is controlled by the solute concentration gradient, which is a function of the solute concentration in the bottom water and the reaction rate in the sediment. In

general, benthic denitrification can be modeled from bottom water NO_x (and O_2) and the reaction rate in the sediment, often expressed as carbon degradation rate [*Bohlen et al.*, 2012; *Middelburg et al.*, 1996]. Thus, in diffusion-controlled sediments, an increased reaction rate usually leads to an increased flux.

In contrast, the flux of a reactive solute in permeable sediments can be decoupled from the reaction rate. In advection-controlled sediments, bottom water enters the permeable sediment, flows through the pore space, and leaves the sediment again. The pressure gradients at the sediment surface and the permeability determine the volume flow, whereas the reaction rate in the sediment determines how much of a solute is consumed on the passage through the sediment. At low reaction rates, part of the solute leaves the sediment without being consumed, and in this case, the net solute flux depends on the reaction rate. However, for increasing reaction rates the amount of solute that leaves the sediment approaches zero and the net solute flux becomes independent of the reaction rate. In this case, the pore water flow is controlling the net flux and the variability of reaction rates has little effect. The ratio of reaction rate over transport rate, also known as the Damköhler number, describes the state of such transport-reaction systems which can be investigated in more detail using numerical models [*Ahmerkamp et al.*, 2015; *Azizian et al.*, 2015; *Cardenas et al.*, 2008].

In this study, the areal denitrification rate (i.e., N-N_2 net flux) in permeable sediments was well described with a linear function of median grain size, whereas no correlation was found for volumetric denitrification rates and proxies such as organic carbon content, water depth, NO_x, and O_2 concentrations. The dependency on grain size and permeability suggests that areal denitrification in this region is to a large extent controlled by advective pore water transport whereas any change of the already high volumetric denitrification rates has little effect.

4.6. N Loss From the NW African Shelf

The correlation between median grain size and areal denitrification allowed extrapolating the results to larger regional scales using a detailed sediment map for the investigated area of 53,700 km^2. Assuming similar conditions throughout the year a total of 7.1 ($\pm$1.7) $\times 10^{10}$ mol N yr^{-1} is denitrified, which is equivalent to 996 ($\pm$233) kt N yr^{-1}. *Seitzinger and Giblin* [1996] estimated a denitrification rate of 8.7 $\times 10^{10}$ mol N yr^{-1} for an area that is several times larger (274,000 km^2, 0–20°N, and <200 m water depth). Accordingly, the spatially averaged N loss of 3.6 ($\pm$0.9) mmol N m^{-2} d^{-1} in this study is fourfold higher than the estimates of Seitzinger and Giblin (0.87 mmol N m^{-2} d^{-1}). The estimate of Seitzinger and Giblin results from an empirical model based on denitrification measurements that do not consider the role of advective transport in permeable sediments. The high contribution of sands to the total denitrification found in this study (Figure 5) suggests that benthic denitrification from sandy sediments may have been underestimated also by other models [*Middelburg et al.*, 1996] and may contribute more to the global benthic N loss than previously assumed. The uncertainty of N loss from sands for global models has been emphasized recently [*Bohlen et al.*, 2012], and our results underline that there is a need to derive reliable estimates, especially for the large areas of sandy sediments that underlie waters with high NO_x concentrations and high primary production. This includes, for example, the Argentine shelf and the Behring Sea (950,000 and 860,000 km^2 [*National Geophysical Data Center*, 2006]), which already make up 10% of the sandy shelf sediments [*Emery*, 1968].

5. Conclusions

Benthic denitrification was the dominant N-loss process in North-West African shelf and margin sediments. Areal denitrification ranged from 0.8 to 9 mmol N m^{-2} d^{-1} with an average of 3.6 mmol N m^{-2} d^{-1}. Areal denitrification rates in permeable sediments correlated significantly with sediment grain size but not with volumetric denitrification rates or bottom water NO_x. Sediment grain size is a proxy for pore water advection, which controls the benthic flux in permeable sediments. The applicability of grain size as a proxy underlines the fundamentally different mode of solute transport in cohesive and permeable sediments. Further, the empirical relation between grains size and areal denitrification allowed extrapolating the results to an area between 12 and 21°N (10–200 m water depth), for which a detailed sediment map was available. A total benthic N loss via denitrification of 7.1 $\times 10^{10}$ mol N yr^{-1} was estimated, which is equivalent to 995 kt N yr^{-1}. In summary, favorable conditions such as high primary production, high bottom water NO_x, low O_2, and efficient advective pore water transport lead to extensive N loss from permeable sediments off North-West Africa. Considering their widespread occurrence, sandy sediments might play an important but so far neglected role in marine N loss.

References

Ahmerkamp, S., C. Winter, F. Janssen, M. M. M. Kuypers, and M. Holtappels (2015), The impact of bedform migration on benthic oxygen fluxes, *J. Geophys. Res. Biogeosci.*, 120, 2229–2242, doi:10.1002/2015JG003106.

Azizian, M., S. B. Grant, A. J. Kessler, P. L. M. Cook, M. A. Rippy, and M. J. Stewardson (2015), Bedforms as biocatalytic filters: A pumping and streamline segregation model for nitrate removal in permeable sediments, *Environ. Sci. Technol.*, 49(18), 10,993–11,002, doi:10.1021/acs.est.5b01941.

Bohlen, L., A. W. Dale, and K. Wallmann (2012), Simple transfer functions for calculating benthic fixed nitrogen losses and C:N:P regeneration ratios in global biogeochemical models, *Global Biogeochem. Cycles*, 26, GB3029, doi:10.1029/2011GB004198.

Boudreau, B. P. (1997), *Diagenetic Models and Their Implementation: Modelling Transport and Reactions in Aquatic Sediments*, 414 pp., Springer, Berlin.

Boudreau, B. P., et al. (2001), Permeable marine sediments: Overturning an old paradigm, *Eos Trans. AGU*, 82, 133–136, doi:10.1029/EO082i011p00133-01.

Braman, R. S., and S. A. Hendrix (1989), Nanogram nitrite and nitrate determination in environmental and biological-materials by Vanadium (III) reduction with chemi-luminescence detection, *Anal. Chem.*, 61(24), 2715–2718.

Cardenas, M. B., P. L. M. Cook, H. Jiang, and P. Traykovski (2008), Constraining denitrification in permeable wave-influenced marine sediment using linked hydrodynamic and biogeochemical modeling, *Earth Planet. Sci. Lett.*, 275(1–2), 127–137, doi:10.1016/j.epsl.2008.08.016.

Carr, M. E. (2002), Estimation of potential productivity in Eastern Boundary Currents using remote sensing, *Deep Sea Res. Part II*, 49, 59–80.

Chen, J., and M. Strous (2013), Denitrification and aerobic respiration, hybrid electron transport chains and co-evolution, *Biochim. Biophys. Acta Bioenergetics*, 1827(2), 136–144, doi:10.1016/j.bbabio.2012.10.002.

Codispoti, L. A. (2007), An oceanic fixed nitrogen sink exceeding 400 Tg N a^{-1} vs the concept of homeostasis in the fixed-nitrogen inventory, *Biogeosciences*, 4(2), 233–253.

Codispoti, L. A., J. A. Brandes, J. P. Christensen, A. H. Devol, S. W. A. Naqvi, H. W. Paerl, and T. Yoshinari (2001), The oceanic fixed nitrogen and nitrous oxide budgets: Moving targets as we enter the anthropocene?, *Sci. Mar.*, 65, 85–105.

Dale, A. W., S. Sommer, E. Ryabenko, A. Noffke, L. Bohlen, K. Wallmann, K. Stolpovsky, J. Greinert, and O. Pfannkuche (2014), Benthic nitrogen fluxes and fractionation of nitrate in the Mauritanian oxygen minimum zone (Eastern Tropical North Atlantic), *Geochim. Cosmochim. Acta*, 134, 234–256, doi:10.1016/j.gca.2014.02.026.

Dalsgaard, T., B. Thamdrup, and D. E. Canfield (2005), Anaerobic ammonium oxidation (anammox) in the marine environment, *Res. Microbiol.*, 156(4), 457–464.

de Beer, D., F. Wenzhöfer, T. G. Ferdelman, S. E. Boehme, M. Huettel, J. E. E. van Beusekom, M. E. Böttcher, N. Musat, and N. Dubilier (2005), Transport and mineralization rates in North Sea sandy intertidal sediments, Sylt-Römö Basin, Wadden Sea, *Limnol. Oceanogr.*, 50(1), 113–127.

DeFlaun, M. F., and L. M. Mayer (1983), Relationships between bacteria and grain surfaces in intertidal sediments, *Limnol. Oceanogr.*, 28(5), 873–881, doi:10.4319/lo.1983.28.5.0873.

Devol, A. H. (2015), Denitrification, anammox, and N2 production in marine sediments, *Annu. Rev. Mar. Sci.*, 7(1), 403–423, doi:10.1146/annurev-marine-010213-135040.

Diester-Haass, L., and P. Müller (1979), Processes influencing sand fraction composition and organic matter content in surface sediments off W Africa (12–19°N), *Meteor-Forschung*, 31, 21–48.

Domain, F. (1977), *Carte Sédimentologique du Plateau Continental Sénégambien: Extension à une Partie du Plateau Continental de la Mauritanie et de la Guinée Bissau*, 18 pp., ORSTOM, Paris.

Domain, F., and B. Richer de Forges (1985), *Carte Sédimentologique du Plateau Continental Mauritanien (entre le cap Blanc et 17°N) à 1: 200 000: Feuilles Nouadhibou et Nouakchott*, 14 pp., ORSTOM, Paris.

Emery, K. O. (1968), Relict sediments on continental shelves of world, *Am. Assoc. Petrol. Geol. Bull.*, 52(3), 445–464.

Engström, P., C. R. Penton, and A. H. Devol (2009), Anaerobic ammonium oxidation in deep-sea sediments off the Washington margin, *Limnol. Oceanogr.*, 54, 1643–1652.

Evrard, V., R. Glud, and P. M. Cook (2012), The kinetics of denitrification in permeable sediments, *Biogeochemistry*, 113(1), 563–572, doi:10.1007/s10533-012-9789-x.

Gao, H., F. Schreiber, G. Collins, M. M. Jensen, J. E. Kostka, G. Lavik, D. de Beer, H.-y. Zhou, and M. M. M. Kuypers (2010), Aerobic denitrification in permeable Wadden Sea sediments, *ISME J*, 4(3), 417–426.

Gao, H., et al. (2012), Intensive and extensive nitrogen loss from intertidal permeable sediments of the Wadden Sea, *Limnol. Oceanogr.*, 57(1), 185–198, doi:10.4319/lo.2012.57.1.0185.

Gihring, T. M., A. Canion, A. Riggs, M. Huettel, and J. E. Kostka (2010), Denitrification in shallow, sublittoral Gulf of Mexico permeable sediments, *Limnol. Oceanogr.*, 55, 43–54.

Ginestet, P., J. M. Audic, V. Urbain, and J. C. Block (1998), Estimation of nitrifying bacterial activities by measuring oxygen uptake in the presence of the metabolic inhibitors allylthiourea and azide, *Appl. Environ. Microbiol.*, 64, 2266–2268.

Grasshoff, K., and H. Johannsen (1972), New sensitive and direct method for automatic determination of ammonia in sea-water, *J. Conseil.*, 34, 516–521.

Grasshoff, K., K. Kremling, and M. Ehrhardt (1999), *Methods of Seawater Analysis*, 3rd ed., Wiley-VCH, Weinheim, New York.

Gruber, N. (2004), The dynamics of the marine nitrogen cycle and its influence on atmospheric CO2 variations, in *The Ocean Carbon Cycle and Climate*, edited by M. Follows and T. Oguz, pp. 97–148, Kluwer Acad., Dordrecht.

Gruber, N., and J. N. Galloway (2008), An Earth-system perspective of the global nitrogen cycle, *Nature*, 451(7176), 293–296, doi:10.1038/nature06592.

Helly, J. J., and L. A. Levin (2004), Global distribution of naturally occurring marine hypoxia on continental margins, *Deep Sea Res. Part I*, 51, 1159–1168, doi:10.1016/j.dsr.2004.03.009.

Holmes, R. M., A. Aminot, R. Kerouel, B. A. Hooker, and B. J. Peterson (1999), A simple and precise method for measuring ammonium in marine and freshwater ecosystems, *Can. J. Fish. Aquat. Sci.*, 56(10), 1801–1808.

Holtappels, M., G. Lavik, M. M. Jensen, and M. M. M. Kuypers (2011), ^{15}N-labeling experiments to dissect the contributions of heterotrophic denitrification and anammox to nitrogen removal in the OMZ waters of the ocean, in *Methods in Enzymology*, edited by G. K. Martin, pp. 223–251, Academic Press, San Diego, Calif.

Holz, C., J. B. W. Stuut, and R. Henrich (2004), Terrigenous sedimentation processes along the continental margin off NW Africa: Implications from grain-size analysis of seabed sediments, *Sedimentology*, 51, 1145–1154, doi:10.1111/j.1365-3091.2004.00665.x.

Huettel, M., and G. Gust (1992), Impact of bioroughness on interfacial solute exchange in permeable sediments, *Mar. Ecol. Prog. Ser.*, 89(2–3), 253–267, doi:10.3354/meps089253.

Huettel, M., and A. Rusch (2000), Transport and degradation of phytoplankton in permeable sediment, *Limnol. Oceanogr.*, *45*(3), 534–549.

Huettel, M., H. Røy, E. Precht, and S. Ehrenhauss (2003), Hydrodynamical impact on biogeochemical processes in aquatic sediments, *Hydrobiologia*, *494*(1), 231–236.

Huettel, M., P. Berg, and J. E. Kostka (2014), Benthic exchange and biogeochemical cycling in permeable sediments, *Annu. Rev. Mar. Sci.*, *6*(1), 23–51, doi:10.1146/annurev-marine-051413-012706.

Jaeschke, A., B. Abbas, M. Zabel, E. C. Hopmans, S. Schouten, and J. S. S. Damste (2010), Molecular evidence for anaerobic ammonium-oxidizing (anammox) bacteria in continental shelf and slope sediments off northwest Africa, *Limnol. Oceanogr.*, *55*, 365–376, doi:10.4319/lo.2010.55.1.0365.

Janssen, F., P. Faerber, M. Huettel, V. Meyer, and U. Witte (2005), Pore-water advection and solute fluxes in permeable marine sediments (I): Calibration and performance of the novel benthic chamber system Sandy, *Limnol. Oceanogr.*, *50*(3), 768–778.

Janssen, F., M. B. Cardenas, A. H. Sawyer, T. Dammrich, J. Krietsch, and D. de Beer (2012), A comparative experimental and multiphysics computational fluid dynamics study of coupled surface-subsurface flow in bed forms, *Water Resour. Res.*, *48*, W08514, doi:10.1029/2012WR011982.

Kessler, A. J., R. N. Glud, M. B. Cardenas, M. Larsen, M. F. Bourke, and P. L. M. Cook (2012), Quantifying denitrification in rippled permeable sands through combined flume experiments and modeling, *Limnol. Oceanogr.*, *57*, 1217–1232, doi:10.4319/lo.2012.57.4.1217.

Krumbein, W. C., and G. D. Monk (1943), Permeability as a function of the size parameters of unconsolidated sand, *Trans. AIME*, *151*, 153–163, doi:10.2118/943153-G.

Le Loeuff, P., and R. von Cosel (1998), Biodiversity patterns of the marine benthic fauna on the Atlantic coast of tropical Africa in relation to hydroclimatic conditions and paleogeographic events, *Acta Oecol. Int. J. Ecol.*, *19*, 309–321.

Marchant, H. K., G. Lavik, M. Holtappels, and M. M. M. Kuypers (2014), The fate of nitrate in intertidal permeable sediments, *PLoS One*, *9*, e104517, doi:10.1371/journal.pone.0104517.

Marchant, H. K., M. Holtappels, G. Lavik, S. Ahmerkamp, C. Winter, and M. M. M. Kuypers (2016), Coupled nitrification–denitrification leads to extensive N loss in subtidal permeable sediments, *Limnol. Oceanogr.*, doi:10.1002/lno.10271.

Meysman, F. J. R., E. S. Galaktionov, B. Gribsholt, and J. J. Middelburg (2006a), Bioirrigation in permeable sediments: Advective pore-water transport induced by burrow ventilation, *Limnol. Oceanogr.*, *51*, 142–156.

Meysman, F. J. R., O. S. Galaktionov, B. Gribsholt, and J. J. Middelburg (2006b), Bio-irrigation in permeable sediments: An assessment of model complexity, *J. Mar. Res.*, *64*, 589–627, doi:10.1357/002224006778715757.

Middelburg, J. J., K. Soetaert, P. M. J. Herman, and C. H. R. Heip (1996), Denitrification in marine sediments: A model study, *Global Biogeochem. Cycles*, *10*(4), 661–673, doi:10.1029/96GB02562.

National Geophysical Data Center (2006), 2-minute Gridded Global Relief Data (ETOPO2) v2. National Geophysical Data Center, NOAA.

Nielsen, L. P. (1992), Denitrification in sediment determined from nitrogen isotope pairing, *FEMS Microbiol. Ecol.*, *86*(4), 357–362.

Polerecky, L., U. Franke, U. Werner, B. Grunwald, and D. de Beer (2005), High spatial resolution measurement of oxygen consumption rates in permeable sediments, *Limnol. Oceanogr. Methods*, *3*, 75–85.

Rao, A. M. F., M. J. McCarthy, W. S. Gardner, and R. A. Jahnke (2007), Respiration and denitrification in permeable continental shelf deposits on the South Atlantic Bight: Rates of carbon and nitrogen cycling from sediment column experiments, *Cont. Shelf Res.*, *27*, 1801–1819, doi:10.1016/j.csr.2007.03.001.

Rao, A. M. F., M. J. McCarthy, W. S. Gardner, and R. A. Jahnke (2008), Respiration and denitrification in permeable continental shelf deposits on the South Atlantic Bight: N2: Ar and isotope pairing measurements in sediment column experiments, *Cont. Shelf Res.*, *28*, 602–613, doi:10.1016/j.csr.2007.11.007.

Rysgaard, S., and R. N. Glud (2004), Anaerobic N$_2$ production in Arctic sea ice, *Limnol. Oceanogr.*, *49*, 86–94.

Santos, I. R., B. D. Eyre, and R. N. Glud (2012a), Influence of porewater advection on denitrification in carbonate sands: Evidence from repacked sediment column experiments, *Geochim. Cosmochim. Acta*, *96*, 247–258, doi:10.1016/j.gca.2012.08.018.

Santos, I. R., B. D. Eyre, and M. Huettel (2012b), The driving forces of porewater and groundwater flow in permeable coastal sediments: A review, *Estuarine Coastal Shelf Sci.*, *98*, 1–15, doi:10.1016/j.ecss.2011.10.024.

Seitzinger, S. P. (1988), Denitrification in freshwater and coastal marine ecosystems: Ecological and geochemical significance, *Limnol. Oceanogr.*, *33*, 702–724.

Seitzinger, S. P., and A. E. Giblin (1996), Estimating denitrification in North Atlantic continental shelf sediments, *Biogeochemistry*, *35*(1), 235–260.

Soetaert, K., P. M. J. Herman, and J. J. Middelburg (1996), A model of early diagenetic processes from the shelf to abyssal depths, *Geochim. Cosmochim. Acta*, *60*(6), 1019–1040.

Soetaert, K., J. J. Middelburg, P. M. J. Herman, and K. Buis (2000), On the coupling of benthic and pelagic biogeochemical models, *Earth Sci. Rev.*, *51*(1-4), 173–201.

Sokoll, S., M. Holtappels, P. Lam, G. Collins, M. Schlüter, G. Lavik, and M. M. M. Kuypers (2012), Benthic nitrogen loss in the Arabian Sea off Pakistan, *Front. Microbiol.*, *3*, 395–412, doi:10.3389/fmicb.2012.00395.

Thamdrup, B., and T. Dalsgaard (2002), Production of N$_2$ through anaerobic ammonium oxidation coupled to nitrate reduction in marine sediment, *Appl. Environ. Microbiol.*, *68*, 1312–1318.

Volkenborn, N., L. Polerecky, D. S. Wethey, and S. A. Woodin (2010), Oscillatory porewater bioadvection in marine sediments induced by hydraulic activities of Arenicola marina, *Limnol. Oceanogr.*, *55*(3), 1231–1247, doi:10.4319/lo.2010.55.3.1231.